Report on MVIRI Aerosol demonstration dataset

Marta Luffarelli (1), Frank Rüthrich (2), Yves Govaerts (1), Viju John (2)

1-Rayference, 2-EUMETSAT

8/21/2019

FIDUCEO has received funding from the European Union's Horizon 2020 Programme for Research and Innovation, under Grant Agreement no. 638822

Contents

1 Introduction

1.1 Scope

This document forms the deliverable D5.8 to report on the climate data record (CDR) of aerosol optical thickness (AOT) as retrieved from the MVIRI fundamental climate data record (FCDR) [RD 1, RD 2, RD 3] using the Combined Inversion of Surface and AeRosol (CISAR) Algorithm [RD 4]. The primary objective of this data record is to assess and demonstrate how the recalibrated and uncertainty-quantified MVIRI FCDR can support improved retrieval of geophysical parameters. Of particular interest is the impact of in-flight reconstructed and spectrally degrading spectral response functions.

1.2 Version Control

Version	Reason	Reviewer	Date of Issue
1.a	Draft structure	Marta Luffarelli	June 2019
1.b	FIDUCEO delivery	Frank Rüthrich and Viju John	23/08/2019
1.0	First release	RPhipps	27/08/2019

1.3 Applicable and Reference Documents

RD 1. Govaerts, Yves; Rüthrich, Frank, John, Viju; Quast, Ralf, Climate Data Records from Meteosat First Generation – Part I: Simulation of Accurate Top-Of-Atmosphere Spectral Radiance over Pseudo-Invariant Calibration Sites for the Retrieval of the In-Flight MVIRI/VIS Spectral Response, Remote Sensing 2018, 10(12), 1959; https://doi.org/10.3390/rs10121959.

RD 2. Ralf Quast, Ralf Giering, Yves Govaerts, Frank Rüthrich and Rob Roebeling, Climate Data Records from Meteosat First Generation Part II: Retrieval of the In-Flight Visible Spectral Response, Remote Sens. 2019, 11(5), 480; https://doi.org/10.3390/rs11050480

RD 3. Frank Rüthrich, Viju O. John, Rob A. Roebeling, Ralf Quast, Yves Govaerts, Emma Wooliams and Jörg Schulz, Climate Data Records from Meteosat First Generation Part III: Recalibration and Uncertainty Tracing of the Visible Channel on Meteosat-2–7 Using Reconstructed, Spectrally Changing Response Functions, Remote Sens. 2019, 11(10), 1165; https://doi.org/10.3390/rs11101165.

RD 4. Y. Govaerts, M. Luffarelli, E. Pinat and V. Leroy (2017): MFG/MVIRI SURFACE AND AEROSOL CDR ALGORITHM THEORETICAL BASIS DOCUMENT

RD 5. Govaerts, Y. and Luffarelli, M.: Joint retrieval of surface reflectance and aerosol properties with continuous variation of the state variables in the solution space – Part 1: theoretical concept, Atmos. Meas. Tech., 11, 6589-6603, https://doi.org/10.5194/amt-11-6589-2018, 2018.

RD 6. Rahman, H., B. Pinty, and M. M. Verstraete (1993). Coupled surface-atmosphere reflectance (CSAR) model. 2. Semiempirical surface model usable with NOAA Advanced Very High Resolution Radiometer Data. Journal of Geophysical Research 98(D11), 20,791–20,801.

RD 7. Vermote, E. F., D. Tanre, J. L. Deuze, M. Herman, and J. J. Morcrette (1997). Second simulation of the satellite signal in the solar spectrum, 6s: An overview. IEEE TGARS 35(3), 675–686.

RD 8. Schaaf, C., Z. Wang. MCD43A3 MODIS/Terra+Aqua BRDF/Albedo Daily L3 Global - 500m V006. 2015, distributed by NASA EOSDIS Land Processes DAAC, https://doi.org/10.5067/MODIS/MCD43A3.006

RD 9. Giles, D. M., Sinyuk, A., Sorokin, M. G., Schafer, J. S., Smirnov, A., Slutsker, I., Eck, T. F., Holben, B. N., Lewis, J. R., Campbell, J. R., Welton, E. J., Korkin, S. V., and Lyapustin, A. I. (2019): Advancements in the Aerosol Robotic Network (AERONET) Version 3 database – automated near-real-time quality control algorithm with improved cloud screening for Sun photometer aerosol optical depth (AOD) measurements, Atmos. Meas. Tech., 12, 169-209, https://doi.org/10.5194/amt-12-169-2019.

RD 10. Henderson, B. and Chylek, P.: The effect of spatial resolution on satellite aerosol optical depth retrieval, IEEE T. Geosci. Remote, 43, 1984–1990, https://doi.org/10.1109/TGRS.2005.852078, 2005.

RD 11. Platnick, S., P. Hubanks, K. Meyer, and M. D. King, 2015: MODIS Atmosphere L3 Monthly Product (08_L3). NASA MODIS Adaptive Processing System, Goddard Space Flight Center. http://dx.doi.org/10.5067/MODIS/MOD08_M3.006 (Terra), http://dx.doi.org/10.5067/MODIS/MYD08_M3.006 (Aqua)

1.4 Glossary

Term	Description
AOT	Aerosol optical Thickness from the MVIRI 0.7 µm band
Albedo	Surface Albedo from the MVIRI 0.7 µm band
BHR	BiHemispherical Reflectance
BRF	Bidirectional Reflectance Factor
CISAR	Combined Inversion of Surface and Aerosols
CDR	Climate Data Record
ECMWF	European Centre for Mid-Range Weather Forecasts
FCDR	Fundamental Climate Data Record
GCOS	Global Climate Observing System
LUT	Look-Up-Table
MAE	Mean Absolute Bias
MFG	Meteosat First generation
OE	Optimal Estimation
QI	Quality Indicator
RMSE	Root Mean Square Error
RPV	Rahman-Pinty-Verstraete
RTM	Radiative Transfer Model
SSR	Sensor Spectral Response
TOA	Top-Of-Atmosphere
RECT2LP	Operational MVIRI image data format

2 The MVIRI Aerosol demonstration dataset

2.1 Dataset Definition and Spatiotemporal Coverage

The MVIRI Aerosol and Albedo demonstration dataset contains the aerosol optical thickness (AOT) and the broadband surface albedo (Albedo) as retrieved from the visible channel of the Meteosat Visible and Infrared Imager (MVIRI) operated on board Meteosat First Generation (MFG) spacecrafts. The channel is centred around 0.7 µm but, as illustrated in Figure 1, the spectral coverage of this channel is very broad.

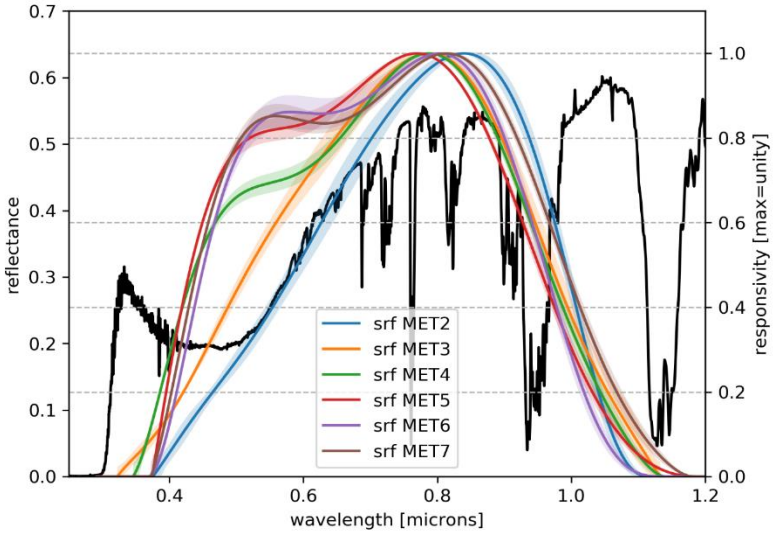

Figure 1: Normalised, reconstructed SRF of MVIRI VIS channel on-board Meteosat-2 to Meteosat-7. Example SCIAMACHY reflectance spectrum is shown in black. The SCIAMACHY spectrum was acquired above Algeria during 2002. Note that the SRFs are subject to spectral degradation and that the herein plotted functions are valid only at the beginning of the operational lifetime of each satellite.

The dataset is produced for 2 of the 7 Meteosat satellites, Meteosat -5 and Meteosat-7, that were operated during the period between 1991 and 2007. While Meteosat-7 was, during the considered period, positioned above 0° longitude, Meteosat-5 was moved from 0° to 63° longitude in support of the INDOEX Experiment in 1998, with continued service in the course of the Indian Ocean Data Coverage (IODC) mission.

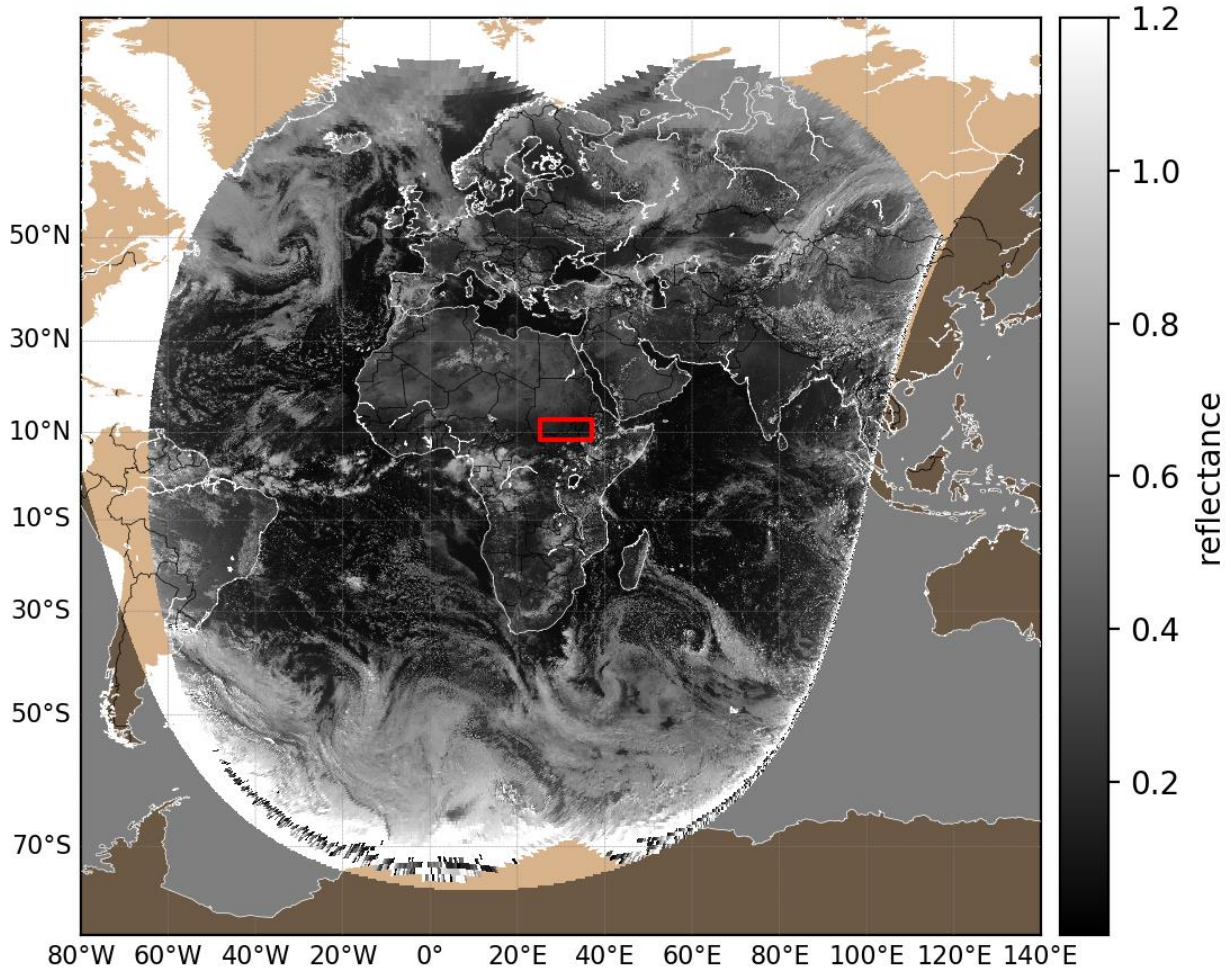

Figure 2: Combined coverage from Meteosat-7 at 0° and Meteosat-5 at 63° on April 2000 at 11:00UTC. The red box indicates the area for the analysis of the time series shown in section 4.

Table 1: Temporal coverage and satellites that are included in the MVIRI Aerosol demonstration dataset

Satellite	Sub-Satellite Longitude	Period
MET5 ZDM	0°	mid 1991-mid 1998 (7y)
MET5 IODC	63°	1998-mid 2007 (5y)
MET7 ZDM	0°	1998-mid 2006 (8y)

2.2 Retrieval Method

The CISAR (Combined Inversion of Surface and Aerosols) algorithm used to produce the MVIRI Aerosol demonstration dataset is described in RD 4. It relies on a joint retrieval of surface reflectance and aerosol optical thickness based on the inversion of a coupled surface-atmosphere radiative transfer model. FASTRE is the forward 1-D Radiative Transfer Model (RTM) used in the CISAR algorithm which divides the observed scene in three layers [RD 5]. The bottom layer is the surface, represented either with the Rahman-Pinty-Verstraete (RPV) model [RD 6] in case of land or with the Cox-Munk model [RD 7] in case of water. The two atmospheric layers are described in Figure 3. FASTRE, is explicitly solved during the inversion process, i.e., it

does not rely on pre-computed solutions, allowing a continuous variation of the state variables in the solution space.

The retrieval scheme is based on an Optimal Estimation (OE) approach where the cost function accounts for the differences between the observations and the forward radiative transfer model, the retrieved state variables and their prior information and finally smoothness constraints on temporal and spectral variations of the aerosol properties.

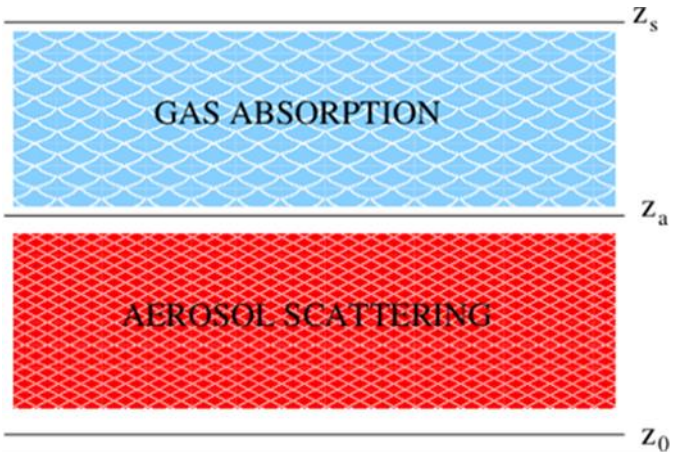

Figure 3: Atmospheric vertical structure of the FASTRE model. The surface is at level Z0 and radiatively coupled with the lower layer L_a extending from level Z_0 to Z_a. This layer includes scattering and absorption processes. The upper layer, L_g, runs from level Z_a to Z_s and only accounts for gas absorption processes (after Govaerts and Luffarelli, 2018).

2.3 Retrieval Uncertainty Propagartion

The OE approach is based on the minimisation of the cost function **J**:

$$J(x) = (F(x) - y)^T S_y^{-1}(F(x) - y) + (x_a - x)^T S_x^{-1}(x_a - x) \qquad \textit{Equation 1}$$

where **x** is the state variable, F(**x**) is the forward model evaluated at **x**, **y** is the multi angular observation vector, $\mathbf{x_a}$ is the prior on the magnitude of the state variable and $\mathbf{S_y}$ and $\mathbf{S_x}$ are the observation and prior covariance uncertainty matrices respectively.

$\boldsymbol{S}_y$ includes the following observation terms:

- the **independent** component of the radiometric error;
- the **structured** component of the radiometric error;
- the **geolocation accuracy** converted into equivalent radiometric error**;**
- the **model parameter** uncertainty converted into equivalent radiometric error;
- the **forward model uncertainty**.

When the cost function has been minimized, the uncertainty U on the retrieved state variable is estimated with:

$$U = (\boldsymbol{K^T S_y^{-1} K + S_x^{-1}}) \qquad \textit{Equation 2}$$

where **K** is the Jacobian matrix, *i.e.* the matrix of the partial derivative of the forward model with respect to the state variables.

2.4 Challenges

The Aerosol/Albedo Algorithm has been used recently to derive AOT and BHR from present-day sensors, such as the Spinning Enhanced Visible and Infrared Imager (SEVIRI) onboard Meteosat Second Generation (MSG) satellites. The application of the algorithm on the much older MVIRI sensor now poses an additional challenge due to several constraints. Among those are the reduced spectral information, the reduced temporal sampling and the spectral degradation of the spectral response function (SRF) in the blue part of the spectrum.

Instead of 3 narrow bands, as the case for SEVIRI, MVIRI only has one very broad visible channel. Monochromaticity, which is an important assumption of the retrieval [RD 4], cannot be expected for this broad band. Thus, a correction has been implemented to account for this [RD 4].

The degrading SRF has been addressed during the generation of the MVIRI VIS FCDR [RD 1, RD 2, RD 3]. The reflectance values that are input to the Albedo/Aerosol retrieval are thus corrected for the changing shape of the SRF. The retrieval itself also considers the changing SRFs. This is possible because the radiative transfer equation is evaluated at runtime, including the convolution with the actual SRF at each time step. The use of reconstructed changing SRFs in the calibration cannot shroud the changing spectral representativeness of the measurements, resulting in expected trends in the time series of Aerosols and Albedo. Those depend on the surface and vary, for the surface albedo, between a decrease of -2.7% over sea and an increase of 8.3% over vegetation (Table 2).

Table 2: Expected change of top of atmosphere (TOA) reflectance, surface albedo and AOT over stable surfaces due to the changing shape of the spectral response function.

	PRE-L.	1998	2005	2014
SEA				
TOA BRF	0.053	0.053	0.051	0.050
TOA BRF	-0.6%		-4.0%	-6.5%
SRF ALB.	0.027	0.027	0.027	0.027
SRF ALB.	-0.4%		-1.6%	-2.7%
VEGETATION				
TOA BRF	0.157	0.158	0.162	0.165
TOA BRF	-1.1%		2.6%	4.3%
SRF ALB.	0.184	0.187	0.197	0.203
SRF ALB.	-1.4%		5.1%	8.3%
DESERT				
TOA BRF	0.359	0.358	0.360	0.362
TOA BRF	0.4%		0.8%	1.3%
SRF ALB.	0.461	0.460	0.468	0.472

SRF ALB.	0.4%		1.7%	2.7%
MEAN AOT	0.171	0.171	0.169	0.167

2.5 Dataset Validation

2.5.1 Validation Data and Method

CISAR retrieves daily AOT and surface BHR_{iso} in the MVIRI VIS band. To validate the Level-2 product, MVIRI observation time series are extracted over selected AERONET stations over 1998-2006 (Table 3). The retrieved BHR and AOT are evaluated against MODIS Shortwave band albedo [RD 8] and AERONET V3 L2 [RD 9] products respectively. Only retrievals with a QI higher or equal to 0.2 are considered in this evaluation.

Table 3 List of selected AERONET stations

AERONET station	Lat	Lon	Land cover
Agoufou	15.345	-1.479	Desert
Alta_Floresta	-9.871	-56.104	Vegetation
Ascension_Island	-7.976	-14.415	Water
Avignon	43.933	4.878	Urban
Bahrain	26.208	50.609	Urban
Banizoumbou	13.541	2.665	Desert
Blida	36.508	2.881	Urban
Cabauw	51.971	4.927	Vegetation
Cabo_da_Roca	38.783	-9.5	Water
Cairo_EMA	30.081	31.29	Urban
Campo_Grande_SONDA	-20.438	-54.538	Vegetation
Capo_Verde	16.733	-22.935	Desert
Carpentras	44.083	5.058	Vegetation
CUIABA-MIRANDA	-15.729	-56.021	Vegetation
Dakar_sea	14.394	-16.959	Water
Dakar_land	14.394	-16.959	Desert
Djougou	9.76	1.599	Mixed
Dunkerque	51.035	2.368	Water
Evora	38.568	-7.912	Urban
FORTH_CRETE	35.333	25.282	Mixed
Granada	37.164	-3.605	Urban
Hamburg	53.568	9.973	Mixed
IER_Cinzana	13.278	-5.934	Mixed
Ilorin	8.32	4.34	Mixed
IMS-METU-ERDEMLI	36.565	34.255	Water
Ispra	45.803	8.627	Vegetation
Izana	28.309	-16.499	Mixed
Karlsruhe	49.093	8.428	Vegetation
Le_Fauga	43.384	1.285	Vegetation
Leipzig	40.335	18.111	Mixed
Mainz	49.999	8.3	Mixed
Modena	44.632	10.945	Urban

Moldova	47	28.816	Urban
Oostende	51.225	2.925	Mixed
Paris	48.867	2.333	Urban
Rome_Tor_Vergata	41.84	12.647	Vegetation
Saada	31.626	-8.156	Vegetation
SEDE_BOKER	30.855	34.782	Desert
Skukuza	-24.992	31.587	Vegetation
Brasilia	-15.601	-47.713	Vegetation
Gobabeb	-23.561	15.042	Desert
Lindenberg	52.21	14.122	Vegetation

2.5.2 Validation Example: The Carpentras Site

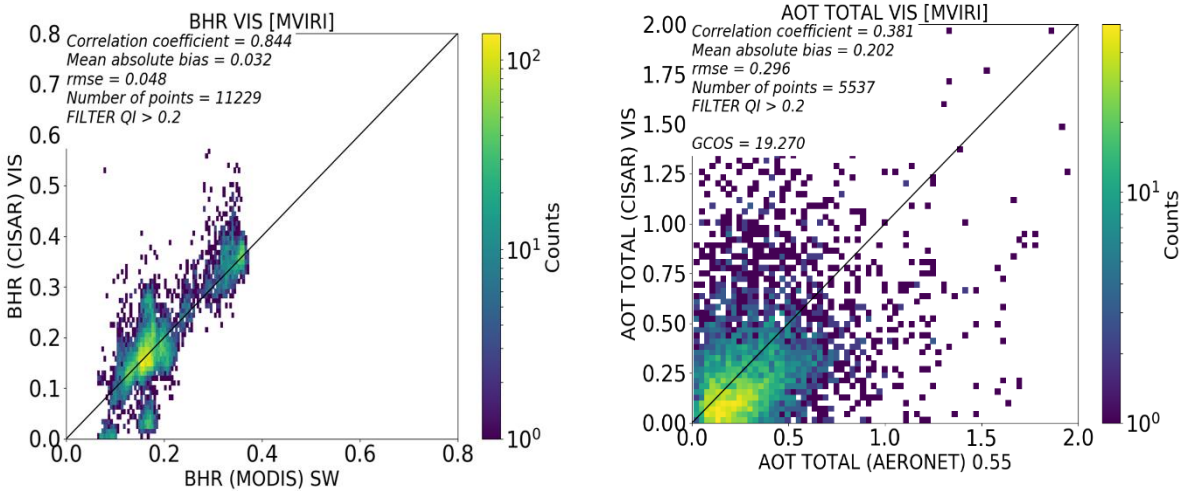

Figure 4 CISAR retrieved BHR_{iso} (left panel) and AOT (right panel) against MODIS Shortwave band albedo and AERONET AOT respectively over all selected targets.

Figure 4 shows the scatterplots between CISAR retrieved surface BHR_{iso} and AOT against the independent datasets, namely MODIS shortwave BHR_{iso} [MCD43A3 Albedo Product V006] and AERONET V3 Level-2 optical thickness. The CISAR retrieval is evaluated in terms of correlation coefficient, Mean Absolute Bias (MAE), Root Mean Square Error (RMSE) and, for the AOT, the percentage of point satisfying the Global Climate Observing System (GCOS) requirements (Systematic Observation Requirements for Satellite-Based Data Products for Climate, 2011 Update), defined as max{0.03,10%}. It can be seen that the surface BHR_{iso} is retrieved fairly accurately, with a correlation of 0.844. Additionally, as can be seen in Figure 5, the BHR_{iso} time series derived from MVIRI/VIS band FCDR over Carpentras, South France, follows the temporal evolution of the surface albedo derived from MODIS. The outliers, for instance at the beginning of 2003 or mid 2004, might be due to errors in the cloud mask data used. Specifically, at the beginning of 2003, CISAR retrieves a BHR of around 0.35 and an AOT of around 1.0. However, for the same day, AERONET data are missing and MODIS data are flagged as bad quality data. This might indicate possible a cloud-contaminated pixel not detected by MVIRI cloud mask. The number of outliers is larger from 2003 to 2006 than in the previous period. This, together with the prior update mechanism on the surface, might explain the increase in the BHR.

Although the surface BHR_{iso} is retrieved quite accurately by CISAR when applied to MVIRI/VIS observations, the aerosol retrieval appears to be more challenging. First, it should be noticed that CISAR is retrieving the AOT in the MVIRI/VIS band, where both important radiative processes, scattering and absorption, take place, while the AERONET product provides the AOT interpolated at 550 nm. Second, the spatial resolution largely differs between the two datasets: CISAR is applied to pixels with a sampling distance ranging from 2.5 km at nadir up to 8 km when the viewing angles are close to 60°, while AERONET data are derived from point measurements. The large spatial resolution of MVIRI pixels has an impact in the aerosol retrieval, as explained by Henderson et al. [RD 10]. Despite these considerations and the consequently large error (RMSE = 0.296), CISAR retrieved AOT shows a moderate positive correlation of 0.38 with the AERONET AOT product.

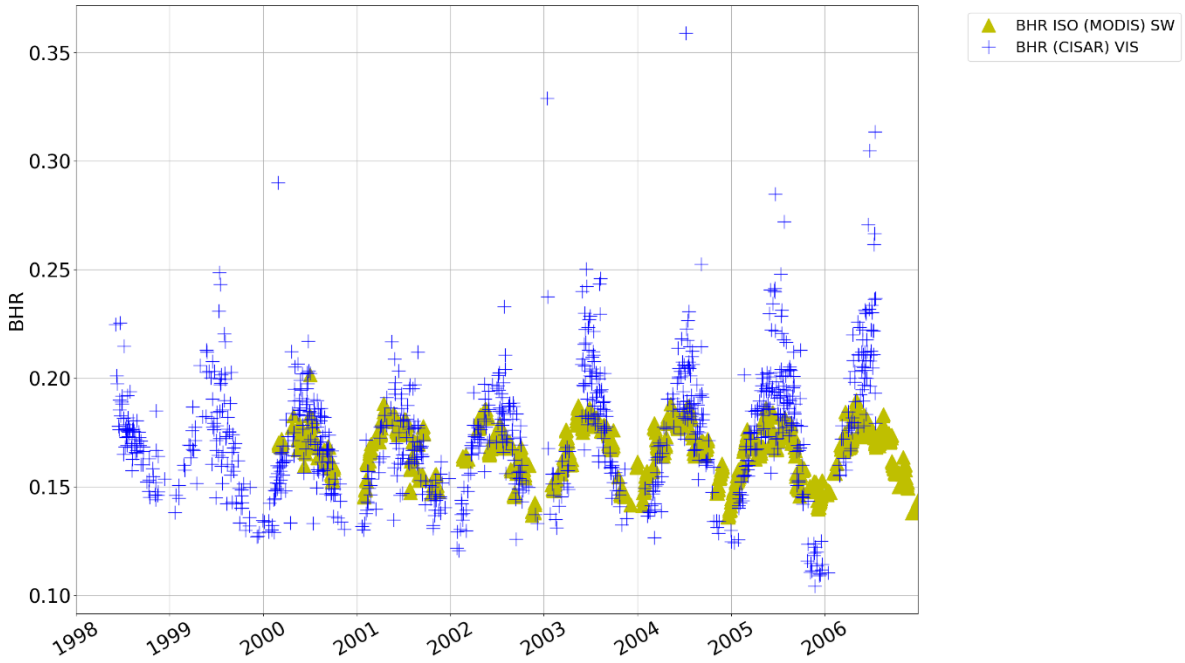

Figure 5 BHR_{iso} timeseries from 1998 to 2006 over Carpentras as retrieved by CISAR from MVIRI VIS band (blue crosses) and as in the albedo Shortwave band MODIS product (yellow triangles). MODIS data are filtered according to the quality mask.

2.5.3 Validation Results for different Land Cover Types

Error! Not a valid bookmark self-reference. and Table 5 report CISAR BHR_{iso} and AOT evaluation, respectively according to the different land cover types (desert, urban, vegetation and coastal). It can be seen that AOT retrieval is particularly challenging over desert, where the main contribution to the Top-Of-Atmosphere Bidirectional Reflectance Factor (TOA BRF) comes from the surface. Over dark surfaces CISAR performs slightly better in retrieving the AOT, showing the best results over water, where the correlation exceeds 0.5 and RMSE=0.173. On the other hand, the surface reflectance retrieval is more accurate over bright surfaces, where it represents the main contribution to the signal. The poor CISAR performances in retrieving the BHR_{iso} over urban areas is partially explained by the pixel spatial heterogeneity over such type of land cover.

Table 4 CISAR BHR_{iso} evaluation against MODIS product according to the different land cover type

	Correlation	Bias	RMSE	Number of points
Desert	0.612	0.03	0.045	1973
Urban	0.103	0.033	0.043	3882
Vegetation	0.477	0.018	0.025	3044

Table 5 CISAR AOT evaluation against AERONET according to the different land cover type

	Correlation	Bias	RMSE	GCOS	Number of points
Desert	0.258	0.334	0.441	9.957	1268
Urban	0.320	0.171	0.230	21.096	1716
Vegetation	0.482	0.194	0.307	22.188	960
Water	0.522	0.117	0.173	29.044	847

2.5.4 Validation of Monthly Averages

The monthly averaged AOT is qualitatively compared with the MODIS combined Dark Target Deep Blue algorithm AOT [RD 11]. As in the case of the evaluation against AERONET, it should be noticed that CISAR retrieves AOT in the MVIRI VIS band, while MODIS algorithm retrieves AOT at 550 nm. Therefore, differences in the magnitude of the retrieved AOT are expected. Nevertheless, AOT patterns are visible in both datasets, such as the biomass burning in central Africa and the dust moving from the Sahara region towards Latin America. Large differences are observed in the Sahara region, where the CISAR retrieval largely overestimates the AOT. The poor performances over desert are in line with what results from the Level-2 validation. Furthermore, the CISAR algorithm is not suitable to perform the retrieval at scenes with ice over water, as here the surface reflectance is computed with the Cox-Munk model taking as input the wind speed

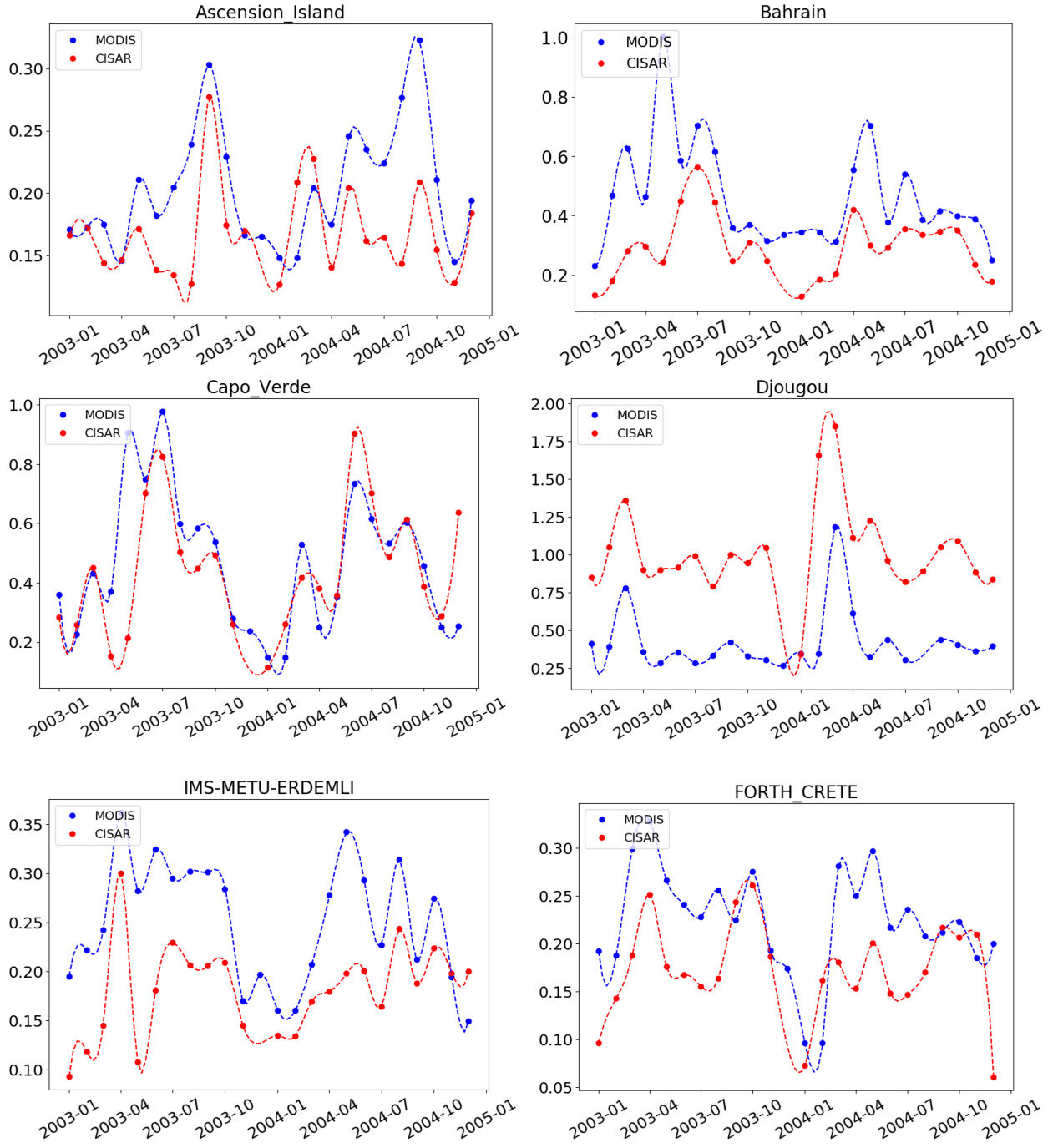

Figure 6 Monthly AOT mean timeseries during 2003 and 2004 over Ascension_Island, Bahrain, Capo_Verde, Djougou, IMS-METU-ERDEMLI, FORTH_CRETE AERONET stations. The blue dots represent the MODIS product, the red ones the CISAR retrieval. The dashed lines represent the cubic interpolation over the MODIS and CISAR datasets.

and direction. This results in a strong underestimation of the surface reflectance and a consequent large overestimation of the AOT.

Despite the differences in magnitude, the CISAR retrieved AOT follows fairly well the temporal evolution of the MODIS product. Figure 6 shows the monthly AOT mean timeseries over 6 AERONET stations for years 2003 and 2004. The MODIS product is displayed in blue, while the CISAR retrieval is displayed in red. The two datasets present a similar temporal evolution of the monthly averaged AOT.

2.6 Uncertainty Validation

The evaluation the Level-2 CISAR uncertainties relies on a Monte Carlo approach applied over 12 of the AERONET stations listed in Table 3 during one year (2004). For each time series, the TOA BRF has been randomly perturbed 100 times within the magnitude of the total observation uncertainty described in Section 2.3. The CISAR algorithm has been applied on each perturbed time series to generate a distribution of solutions. The 12 AERONET stations are selected according to geographic location and land cover type:

- Area 1 (urban/vegetation): Avignon, Carpentras, Le_Fauga
- Area 2 (bright surface): Banizoumbou, Agoufou, Djougou, IER_Cinzana, Ilorin
- Area 3 (coastal): Cabo_da_Roca, El_Arenosillo
- Area 4 (urban/vegetation): Karlsruhe, Mainz

Figure 7 shows an example of the Monte Carlo method to evaluate CISAR uncertainty over Avignon (South France). The distribution of the 100 AOT retrieved with the Monte Carlo method resembles a Gaussian distribution with μ=0.175 and σ=0.051. For the same day, CISAR applied on the non-perturbated satellite observations retrieves an AOT equal to 0.175 with σ=0.118, thus showing a too large uncertainty compared to the Monte Carlo simulations.

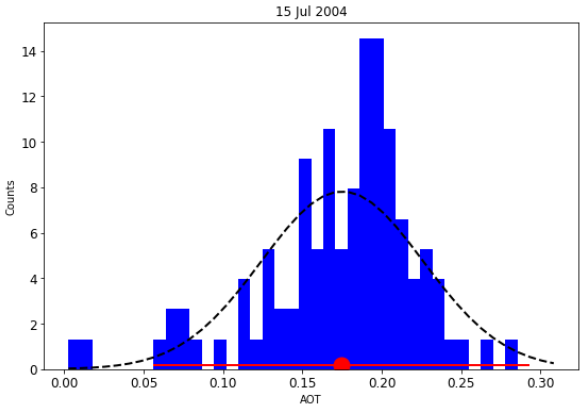

Figure 7 Distribution of the AOT retrieved from the 100 Monte Carlo simulations. The black dashed line represents the resulting normal distribution. The red dot represents the AOT retrieved with no perturbation and the red lines represent its uncertainty.

The results over all the selected stations during the year 2004 are shown in Figure 8. Overall, CISAR uncertainties appear to be larger than the uncertainties estimated with the Monte Carlo method. The scatterplot between the uncertainties obtained with the Monte Carlo simulations and the retrieval uncertainties is similar regardless the land cover type, although over bright surfaces the correlation between the uncertainties obtained with the Monte Carlo method and the CISAR retrieval uncertainty is lower. Considering the non-diagonal elements of the uncertainty covariance matrices might decrease the retrieval uncertainty if the state variables are anticorrelated. The large overestimation is also partially due to the high uncertainty associated with the prior information on the AOT magnitude, given its contribution to the final retrieval uncertainty (Equation 2). Figure 9 shows the relationship between the relative uncertainty and the AOT. It can be seen that the CISAR retrieved uncertainty has a stronger dependency on the AOT. This could be due to the prior uncertainty contribution being constant regardless the magnitude of the retrieve optical thickness. More investigation on this aspect is needed.

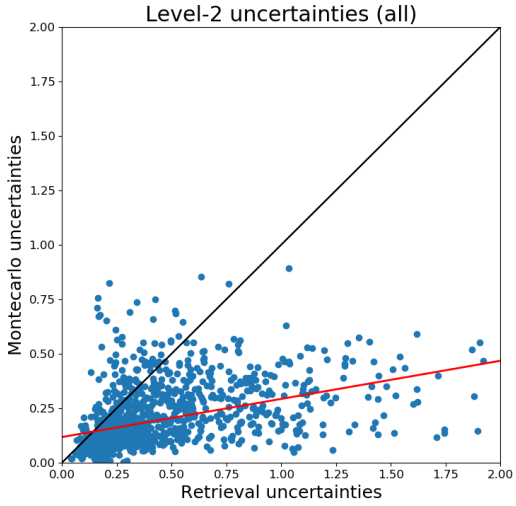

Figure 8 Scatterplot between the sigma of the distribution resulting from Monte Carlo simulations (y axis) and the CISAR retrieved uncertainty on the non-perturbated satellite observations (x axis).

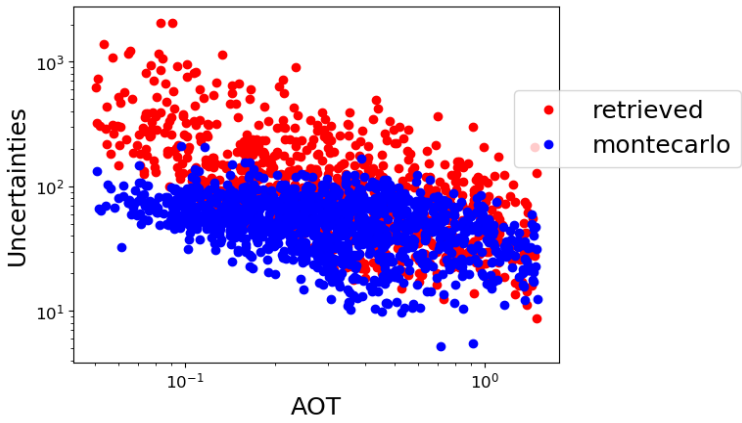

Figure 9 Relative uncertainty magnitude (y axis) in function of the AOT for both the uncertainties retrieved by CISAR (red dots) and the ones obtained with the Monte Carlo method (blue dots).

3 Demonstration of the Impact of the recalibrated FCDR

Within the FIDUCEO project, the MVIRI Sensor Spectral Response (SSR) has been recovered, taking into account its spectral ageing [RD 2]. To assess the impact of the reconstructed SSR, the time series over the AERONET stations listed in Table 3 have been processed twice: firstly based on FCDR format relying on the reconstructed sensor spectral function and secondly based on the original RECT2LP format where data have

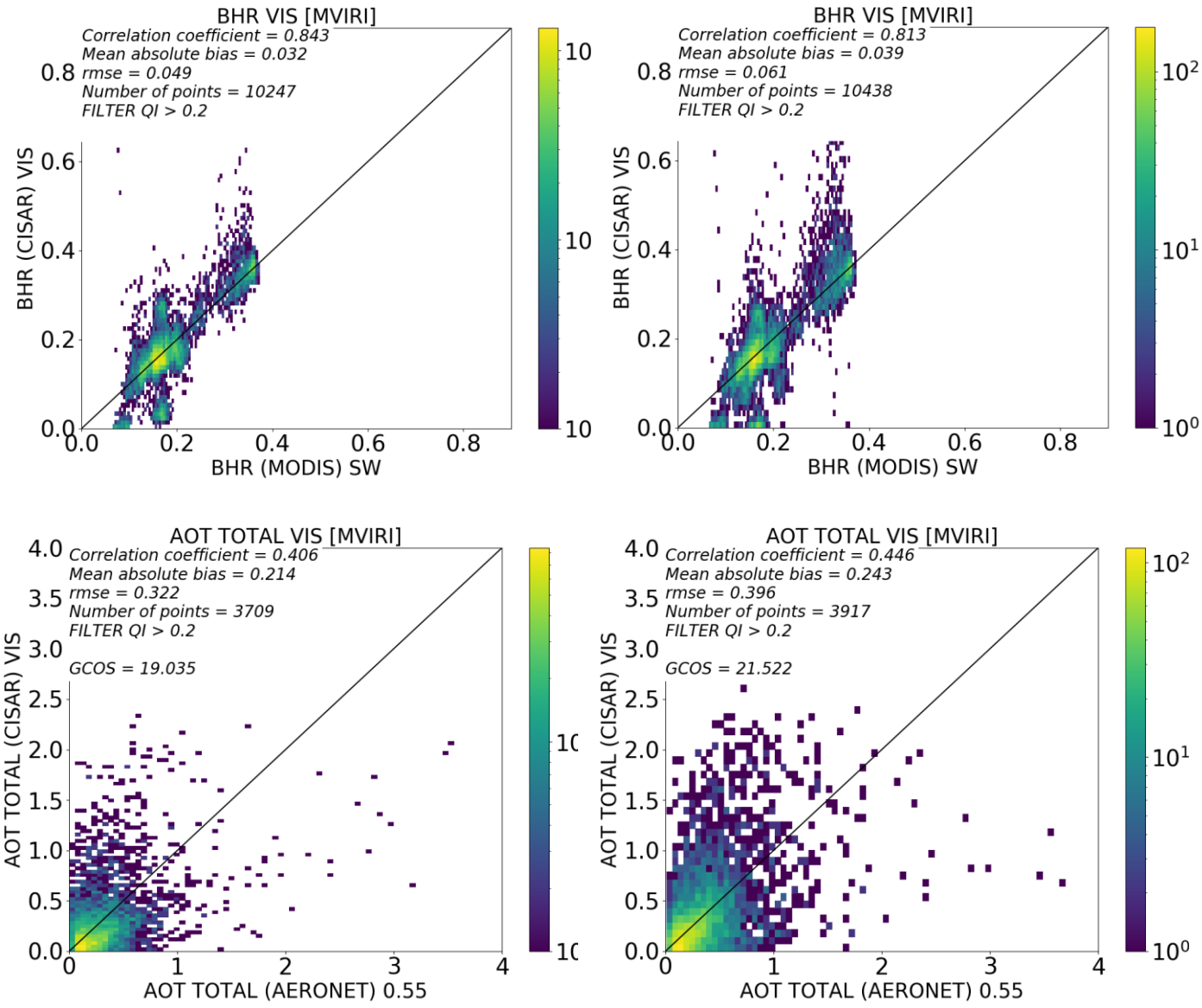

Figure 10 Scatterplots between CISAR retrieved BHR_{iso} (top panel) and AOT (bottom panel) (y axis) against the MODIS Shortwave band albedo and the AERONET product respectively (x axis). In the left panels the retrieval is performed using the reconstructed SSR, in the right ones the original SSR is used.

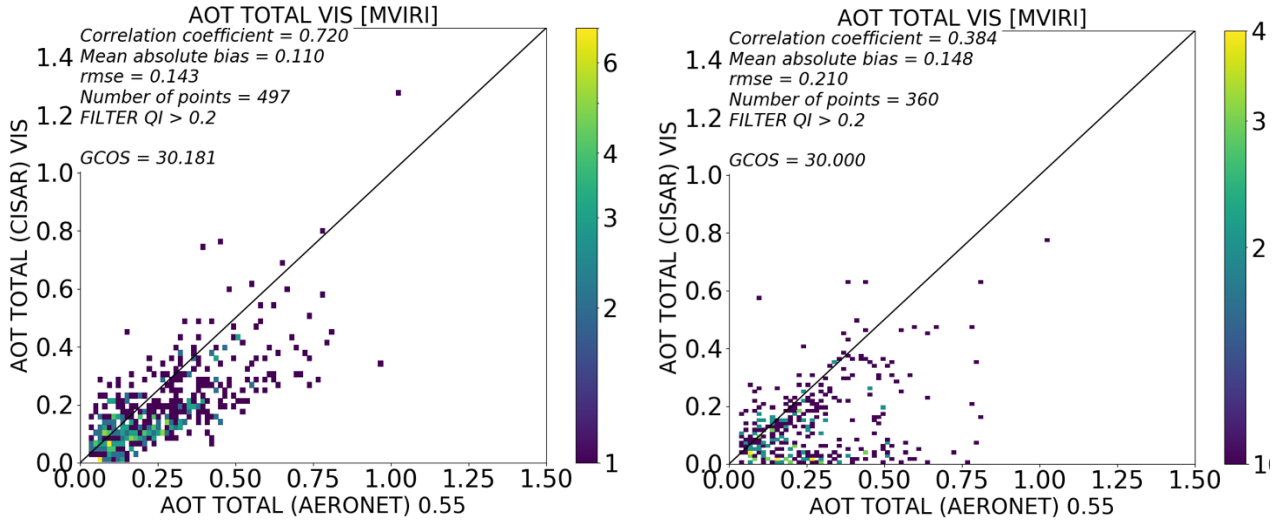

Figure 11 Same as Figure 10 but only over water targets.

been calibrated with the original pre-launch sensor spectral function. Figure 10 shows the evaluation of the BHR_{iso} and AOT retrieved by CISAR against MODIS Shortwave band surface albedo and AERONET products using the FCDR (left panels) and the RECT2LP (right panels) format. The AOT retrieval with the original SSR shows a slightly higher correlation of 0.446 (compared to 0.406 of the retrieval performed considering the reconstructed SSR), but also a larger error; the MAE is 0.243 and the RMSE is equal to 0.396 (compared to 0.214 and 0.322 respectively when the retrieval is performed considering the reconstructed SSR). On the other hand, the surface albedo retrieval worsens both in term of correlation and error. A visual inspection of Figure 10 top panels reveals that the CISAR retrieval based on the RECT2LP data exhibit more scattering with respect to MODIS than with the reconstructed FCDR. Also, more scatter is visible when CISAR is applied considering the original SSR.

The SSR recovery mostly impacted the blue spectral region of the MVIRI/VIS band [RD15]. For this reason, the larger effect of the SSR recovery is expected to take place over water surface, where most of the signal originates from the blue and red spectral regions (Figure 11). In that case, the correlation coefficient between the MVIRI AOT values and the AERONET values increases from 0.38 with the original sensor spectral function up to 0.72 with the reconstructed ones. This example clearly shows the benefit of the FCDR for the retrieval of AOT over water surfaces. Over land surface, the large variability of possible spectral variations of the surface reflectance within the VIS band is a strong limiting factor for the development of an efficient monochromatic assumption correction unlike over water surface where the surface spectral variability can be determined.

4 Time series of AOT and Albedo from Meteosat-5 and -7

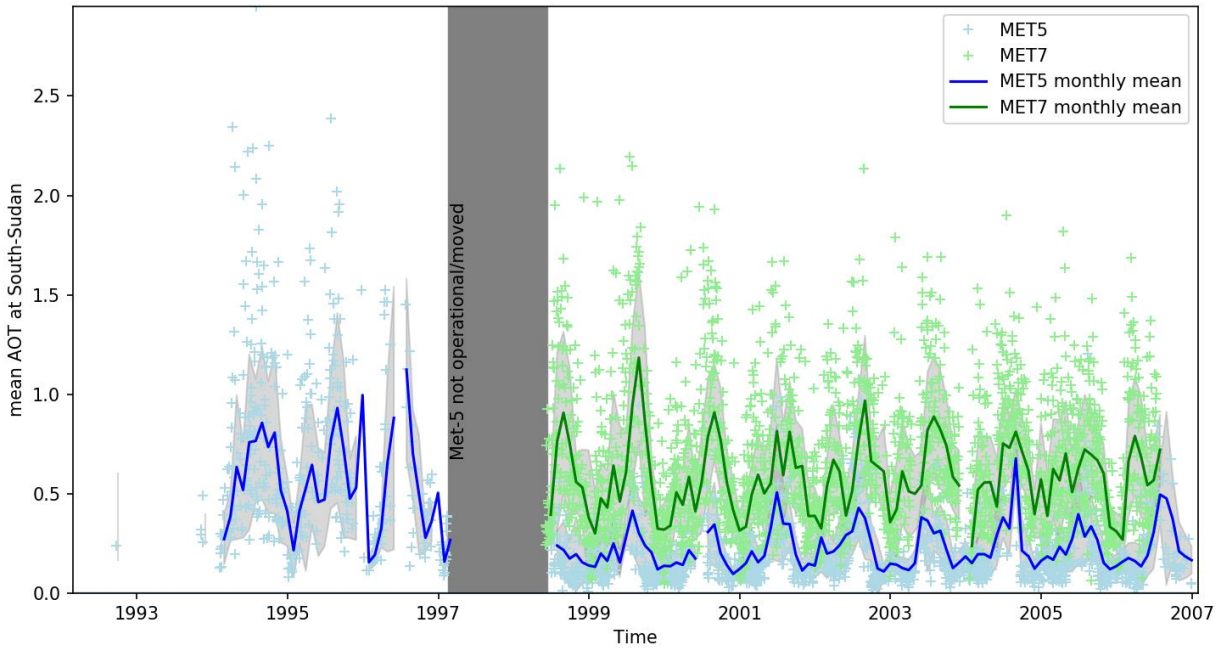

Figure 12: AOT time series averaged over southern Sudan

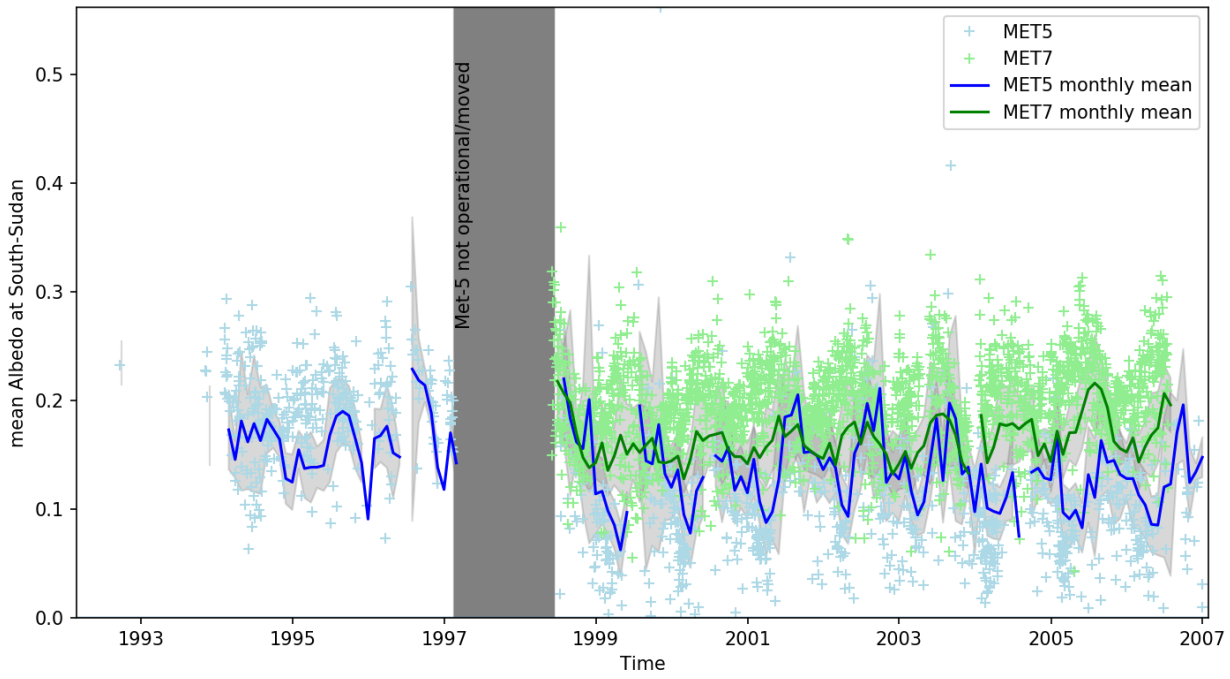

Figure 13: Albedo time series averaged over southern Sudan

As mentioned above, the described retrieval of AOT and Albedo was applied on Meteosat-5 and -7 measurements during the period between 1992 and 2007. Figure 12 demonstrates the temporal variability of the AOT, averaged over the area indicated in Figure 2. The magnitude of the AOT signal derived from both, Meteosat-5 and -7, located at 0° is comparable. For Meteosat-5 this is the time between 1992 and 1998, for Meteosat-7 this is the time between 1998 and 2007. A significant difference exists between the AOT values retrieved from satellites at different sub-satellite points. This is visible for the time after 1998,

where the AOT derived from Meteosat-7 at 0° is up to 100% larger than the AOT derived from Meteosat-5 at 63°. However, despite this difference of the absolute values, the variability with time follows a common pattern for both satellites.

The retrieved Albedo time series is illustrated in Figure 13. The observed patterns are quite similar to the AOT, only the difference between Meteosat-5 and -7 is smaller.

Potential reasons for the difference between the sub-satellite points may be a viewing-geometry dependent performance of the cloud-masking algorithm and the different shapes and levels of degradation of the SRFs of Meteosat-5 and -7.

5 Summary and Conclusion

In the framework of the FIDUCEO project, CISAR has been applied to MVIRI Meteosat images from 1998 to 2006, delivering daily AOT and surface albedo in the MVIRI/VIS band.

The Level-2 product has been evaluated against AERONET and MODIS products over the AERONET stations listed in Table 3, selected according to geographical location and land cover type. The results of this evaluation show that CISAR accurately retrieves surface albedo, with a correlation of 0.844 and a RMSE=0.048, when compared against MODIS Shortwave band albedo product. However, AOT is retrieved with a large error and a moderate positive correlation. The poor performances in retrieving the AOT are mostly due to the non-monochromaticity of the MVIRI/VIS band. Figure 14 illustrates the scattering and absorption processes taking place in that band. Although FASTRE has been modified within the FIDUCEO project to include a correction for the violation of the monochromaticity assumption, over land surface the variability of the surface reflectance spectral shape is too large to implement an efficient correction, limiting thereby the reliability of aerosol retrieval with the inversion of a physically-based radiative transfer model.

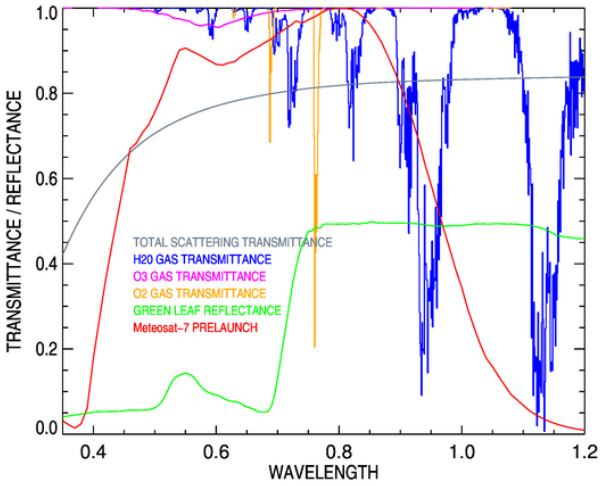

Figure 14 Molecular transmittance in the MVIRI/VIS band spectral range for the following gases: water vapor (blue), ozone (magenta) and oxygen (orange). The grey line shows typical total (Rayleigh and aerosol) scattering transmittance. The green line illustrates the typical reflectance of a green leaf. The red line shows the pre-launch SRF of MVIRI/VIS band on board Meteosat-7. Wavelength is expressed in µm.

Nevertheless, the evaluation of the monthly averaged product shows a good temporal agreement with the MODIS combined Dark Target and Deep Blue product. CISAR also seems to be capable of correctly detecting aerosol events such as biomass burning in central Africa and dust transportation from the Sahara region towards South America and to follow the temporal evolution of the AOT.

An alternative to the monochromatic assumption correction could consist in considering the VIS band as a sum of contributions from the various (VIS/NIR) spectral regions. However, only AVHRR information can provide spectral information within the VIS band during the Meteosat First Generation (MFG) era, but it would require a better calibration of the AVHRR channels during the eighties.

CISAR Level-2 retrieval uncertainties have also been evaluated with the Monte Carlo method applied over 12 AERONET stations over one year of data (2004). The result of this evaluation shows that the Level-2 estimated retrieval uncertainties are larger than expected. This overestimation can be partially explained by the too large contribution of the AOT prior uncertainty, although more investigation is needed. As the Level-

2 retrieval uncertainties do not discriminate among the different sources of uncertainties (common, structured and independent), the propagation to the Level-3 is not straightforward. To associate an uncertainty to the Level-3 product from MVIRI observations the Monte Carlo method has been exploited once again. Monthly means have been computed from the Monte Carlo simulations and averaged over selected areas (over urban, vegetated, bright and coastal/water surfaces) to simulate the re-gridding at 1-degree resolution. The uncertainties of the Level-3 result much smaller than the ones in the Level-2, as the independent component of the uncertainty cancels out when averaging in time and space.

In the course of this report, the impact of the reconstructed SSR of MVIRI/VIS band has been quantified in terms of accuracy of the CISAR retrieval of surface reflectance and AOT. Though the AOT retrieval shows similar performances when CISAR is applied to the FCDR or RECT2LP format, the BHR retrieval deteriorates when the TOA BRF are calibrated with the original SSR. As the blue region of the VIS band was mostly affected by the SSR recovery, the larger impact is visible over water targets, as most of the radiative information over water originates from that spectral region. Over these targets, the AOT retrieval shows a better agreement when compared to the AERONET product when the recovered SSR is used. This opens up the possibility of AOT retrievals over water surfaces before the MODIS era.

A combined Meteosat-5 and -7 time series acquired at the border between Sudan and South-Sudan has been shown. The time-series illustrates well that the retrieved Aerosol and Albedo quantities at this site are in line for both satellites. However, a difference of the sub-satellite longitude, and the subsequent difference of the viewing geometry, seems to lead to substantial differences of the retrieved quantities: During the period between 1998 and 2007 the quantities derived from Meteosat-5, located at 63°E, are significantly lower than those derived from Meteosat-7, located at 0°. The evolutions of AOT and Albedo with time, nevertheless, are in fairly good agreement.